Electronic Supplementary Information

Principle in Interlayer-Spacing Regulation of Layered Vanadium Phosphates for Superior Zinc-ion Batteries

Linfeng Hu*[a,b], Zeyi Wu[b], Chengjie Lu[a], Fei Ye[a], Qiang Liu[a], Zhengming Sun[a]

a. School of Materials Science and Engineering, Southeast University, Nanjing, 211189, China

b. Department of Materials Science, Fudan University, Shanghai 200433, China

* Address correspondence to: linfenghu@seu.edu.cn

Contents:

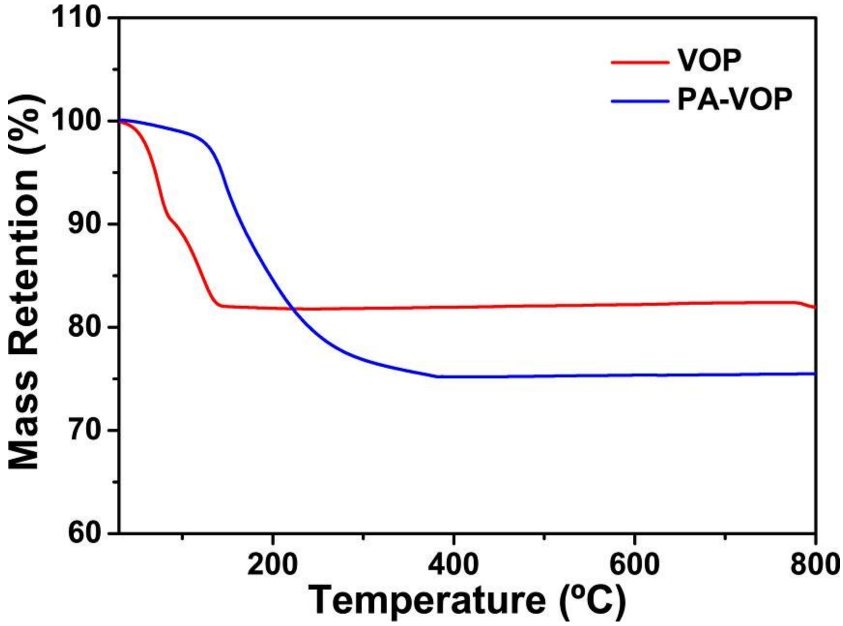

Fig. S1. Thermogravimetric analysis (TGA) curve of VOP and PA-VOP (16.5 Å), respectively.

Moreover, thermo gravimetric analysis (TGA) result reflects a weight loss of 19.2 % before 150 °C of VOP, consistent with two H_2O contained per molecule in VOP, while the weight loss of 25.3 % of PA-VOP indicates 0.6 phenylamine per molecule in PA-VOP. In view of the primary loss before 600 °C, polymerization of the intercalated phenylamine is certainly Infinitesimal.

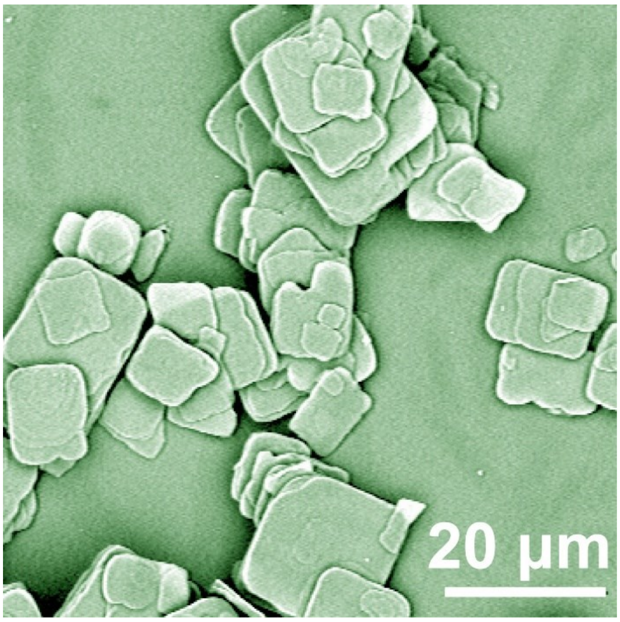

Fig. S2. SEM image of precursor VOP bulk.

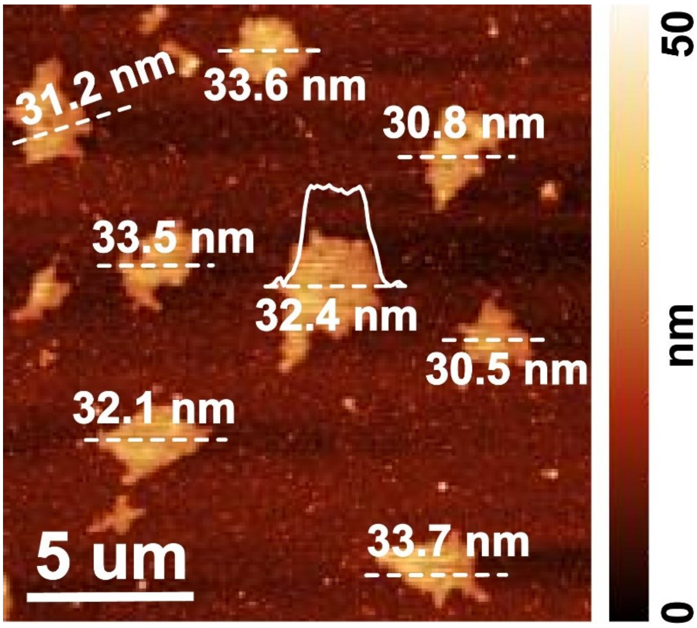

Fig. S3. AFM image of VOP nanoplates precursor. Insert is a typical height curve of an individual nanoplate.

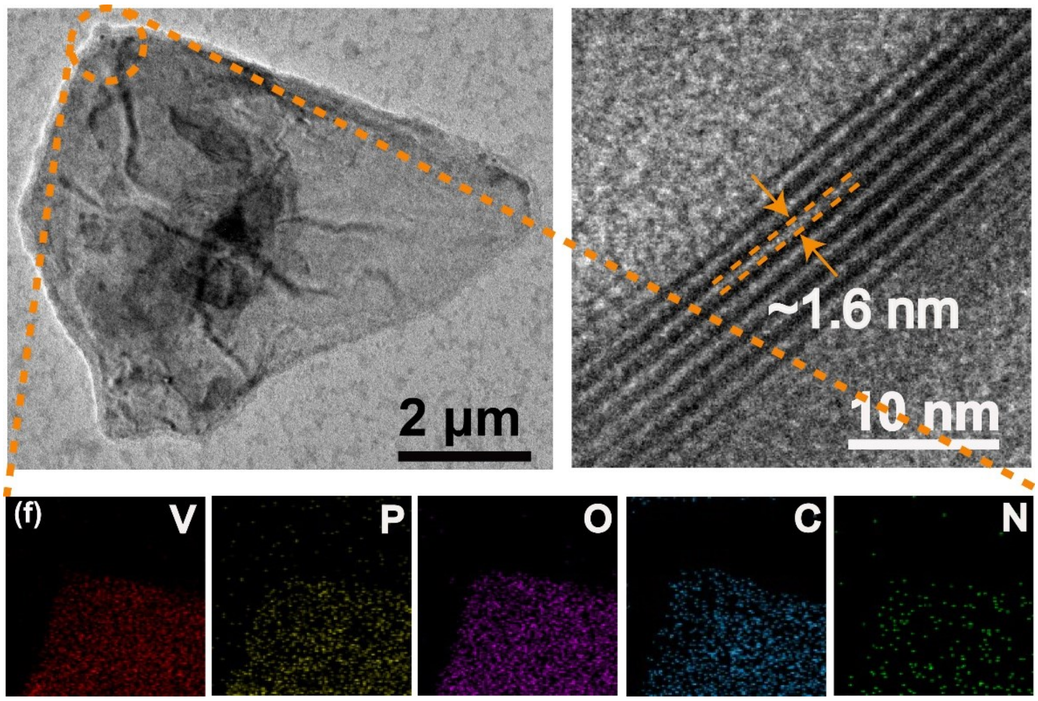

Fig. S4. Typical TEM image, the cross-sectional HRTEM image and corresponding V, P, O, C, N element mapping of an individual PA-VOP sheet.

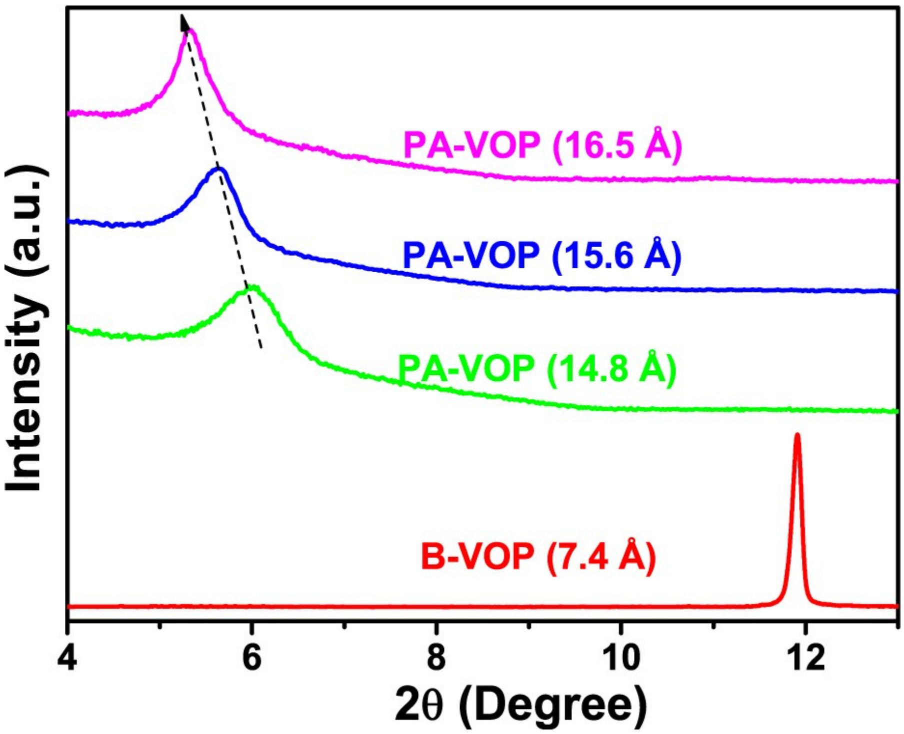

Fig. S5. XRD patterns of various PA-VOP samples synthesized under different temperature and solvent (2θ range : 4°-13°).

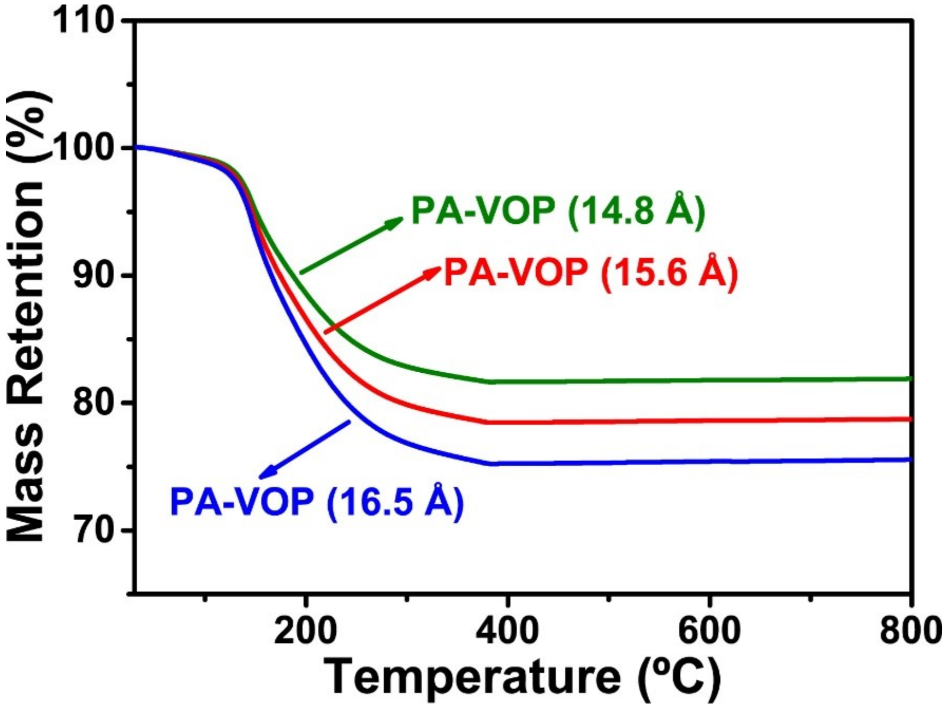

Fig. S6. TGA curves of PA-VOP samples with different interlayer spacing, respectively.

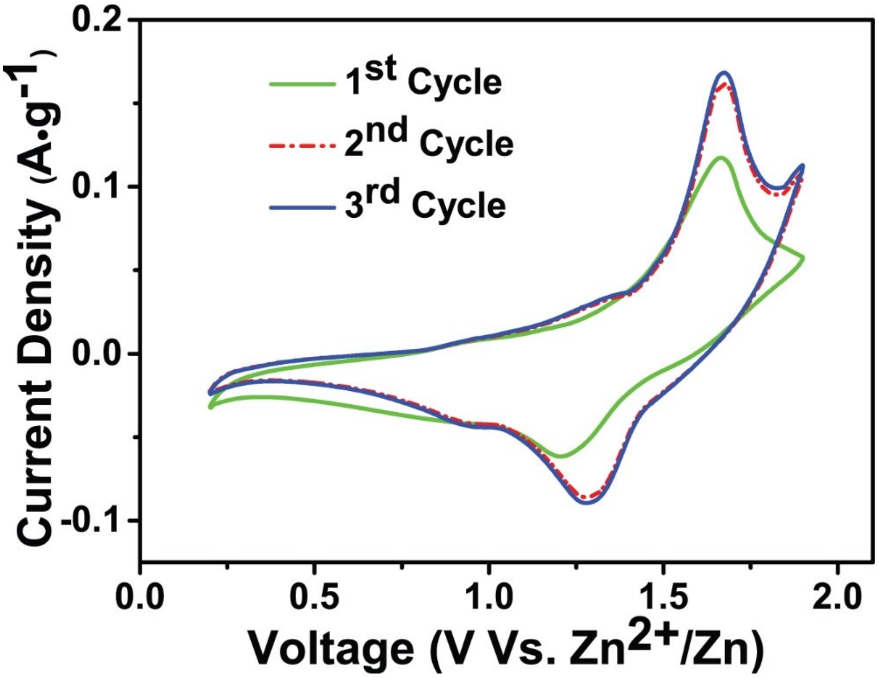

Fig. S7. CV curves of the Zn / PA-VOP (16.5 Å) battery in intial three cycles.

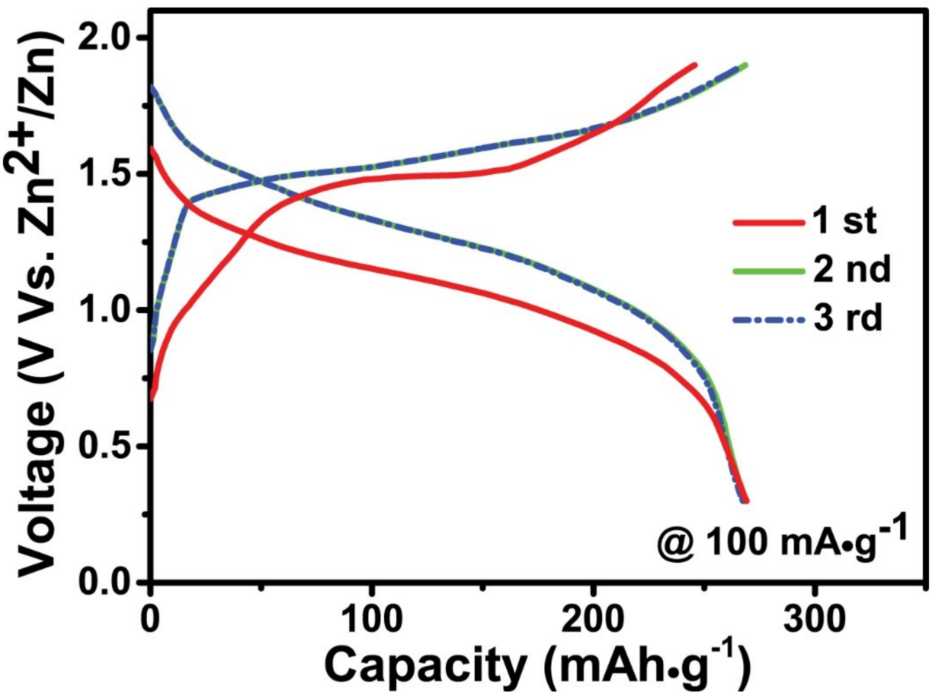

Fig. S8. GCD curves of the Zn / PA-VOP (16.5 Å) battery in intial three cycles.

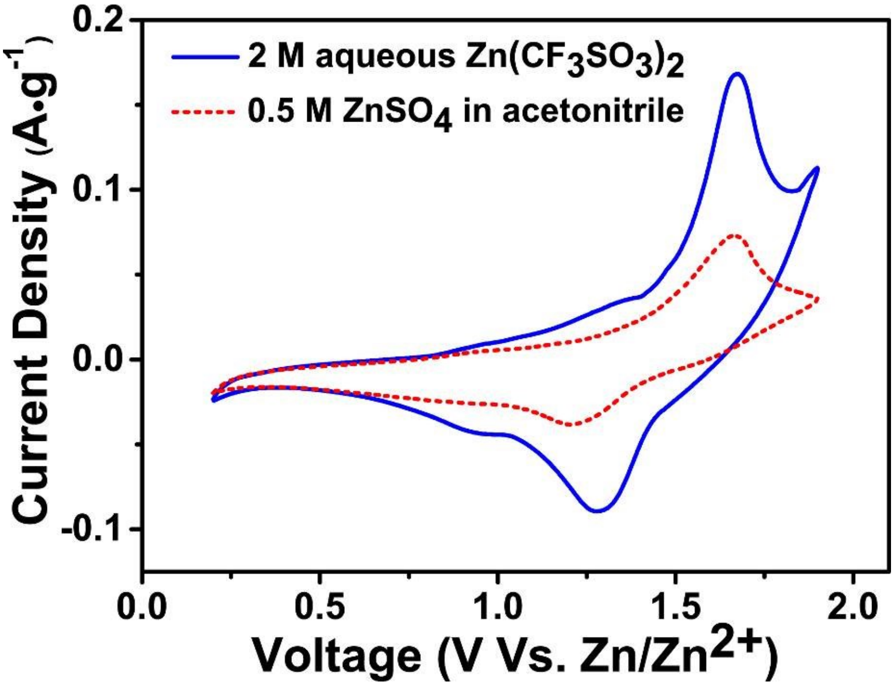

Fig. S9. CV curve of Zn / PA-VOP battery at the scan rate of 0.1 $mV \cdot s^{-1}$ using different electrolyte (aqueous and non-aqueous).

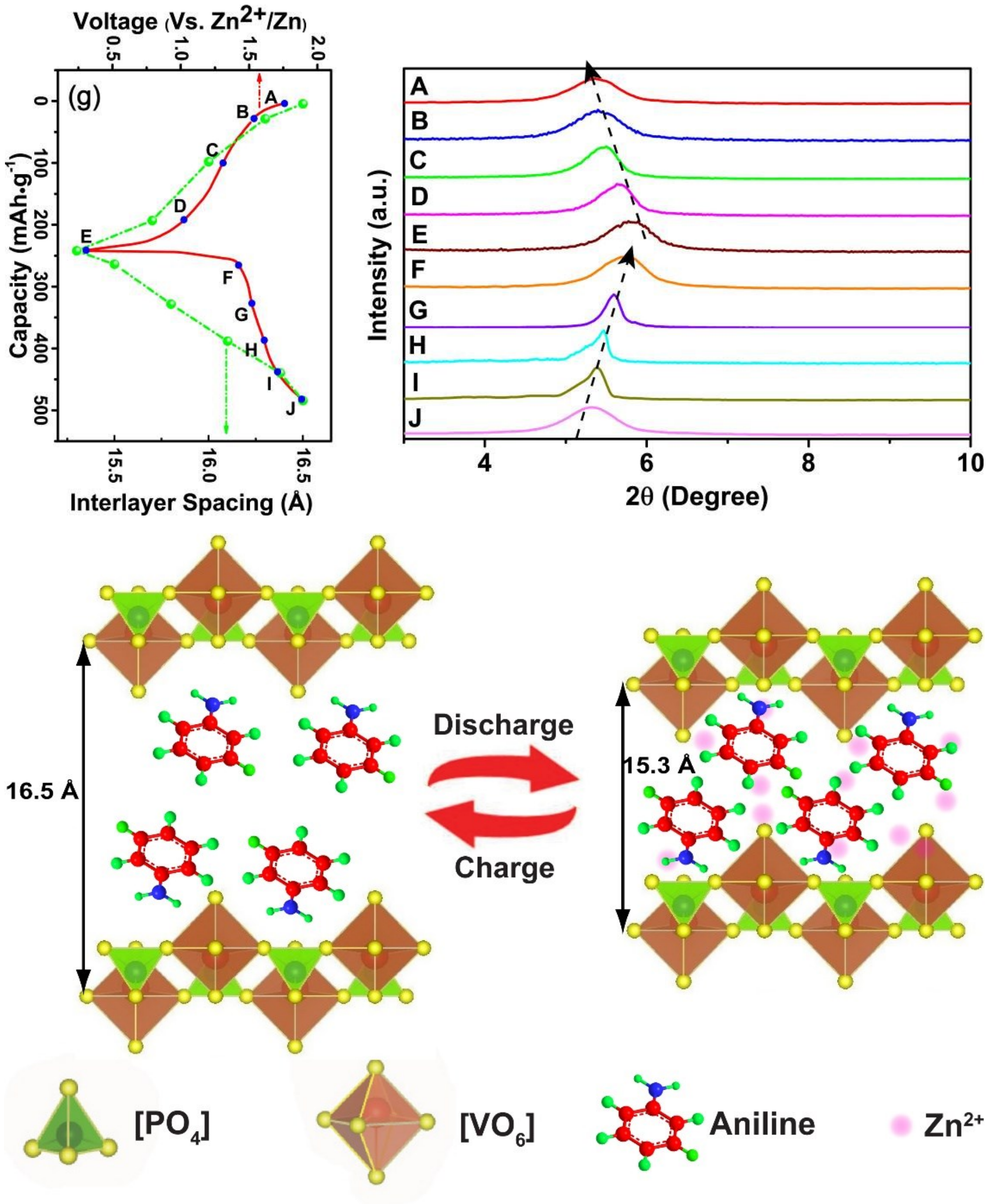

Fig. S10. *Ex-situ* XRD characterization and corresponding scheme of Zinc-ion storage mechanism in PA-VOP cathode.

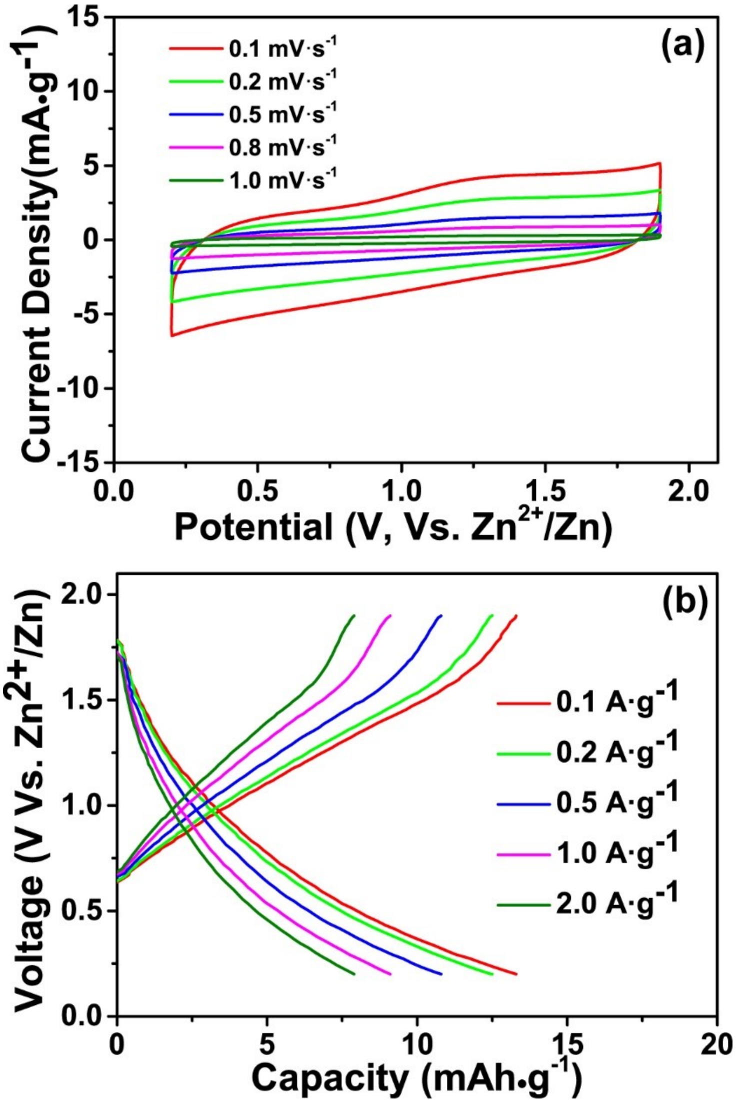

Fig. S11. CV and GCD curves of Zn // PA battery at different scan rate and varied current density, respectively.

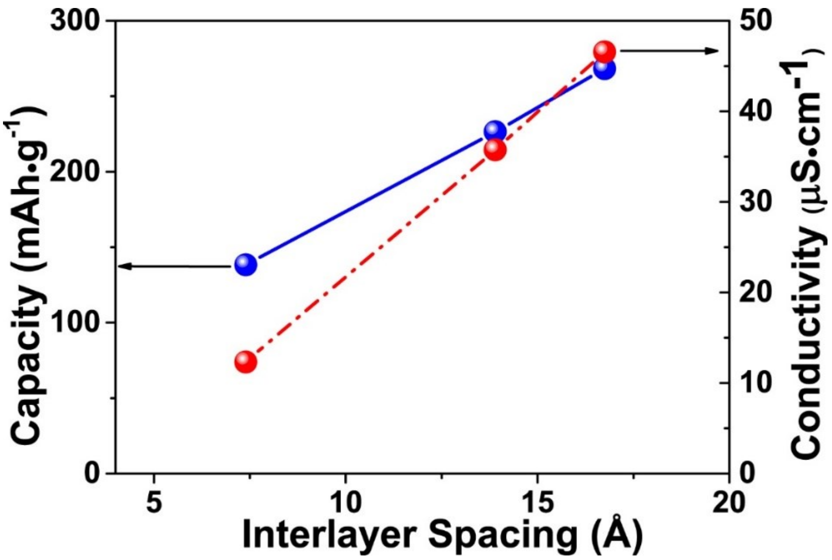

Fig. S12. Dependence between specific capacity, electronic conductivity and the interlayer spacing of various $VOPO_4$-based cathodes.

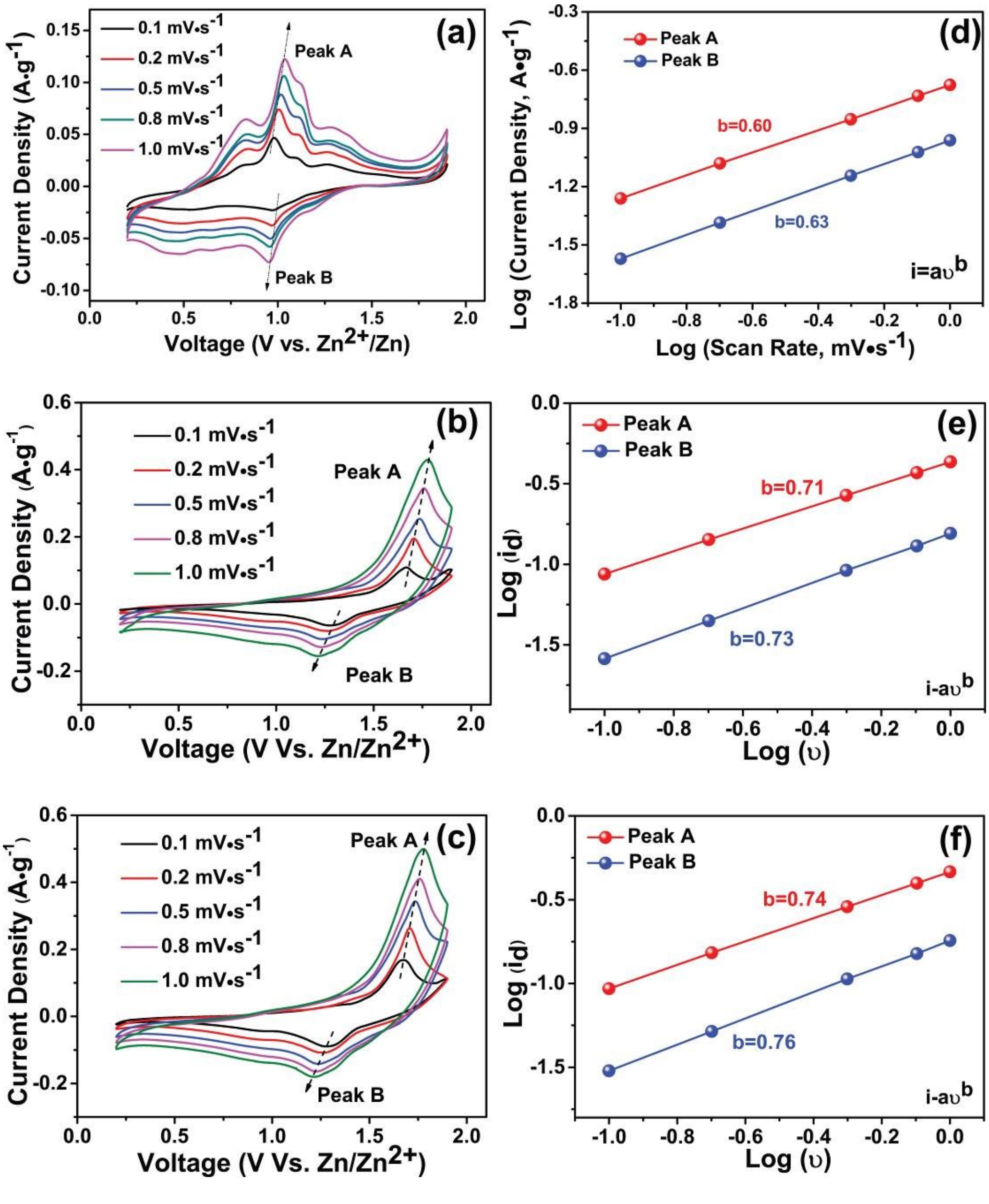

Fig. S13. (**a)-(c)** CV curves of VOP (7.4 Å), PA-VOP (14.8 Å phase) and PA-VOP (16.5 Å phase) cathode at different scan rate and (**d)-(f)** the corresponding dependence of logrithm of peak current density and scan rate, repectively.

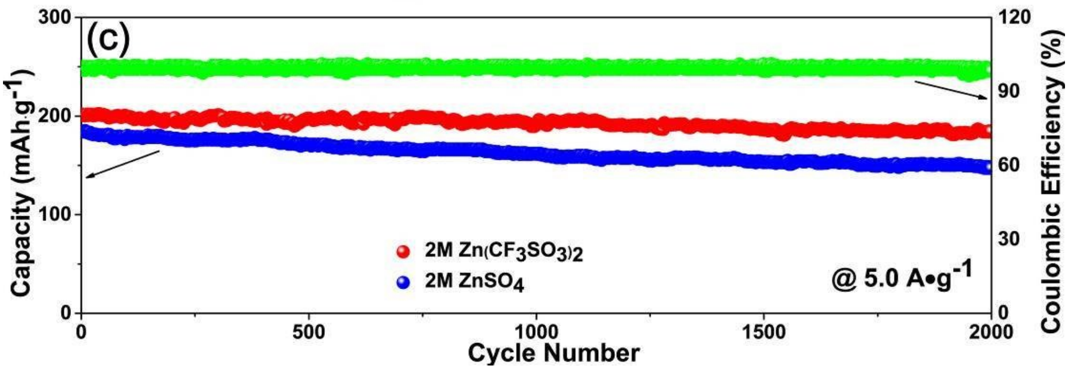

Fig. S14. Cycling performance at 5.0 A·g^{-1}and coulombic efficiency of Zn / PA-VOP coin cells employing 2M $Zn(CF_3SO_3)_2$ and 2M $ZnSO_4$ aqueous solution as electrolyte, respectively. Compared to a capacity loss of 20.3 % in aqueous $Zn(SO_4)_2$ electrolyte, superior lifespan with less capacity decay (7.7%) was observed in $Zn(CF_3SO_3)_2$ electrolyte due to the better desolvation effect of bulky $(CF_3SO_3)^-$ versus $(SO_4)^{2-}$

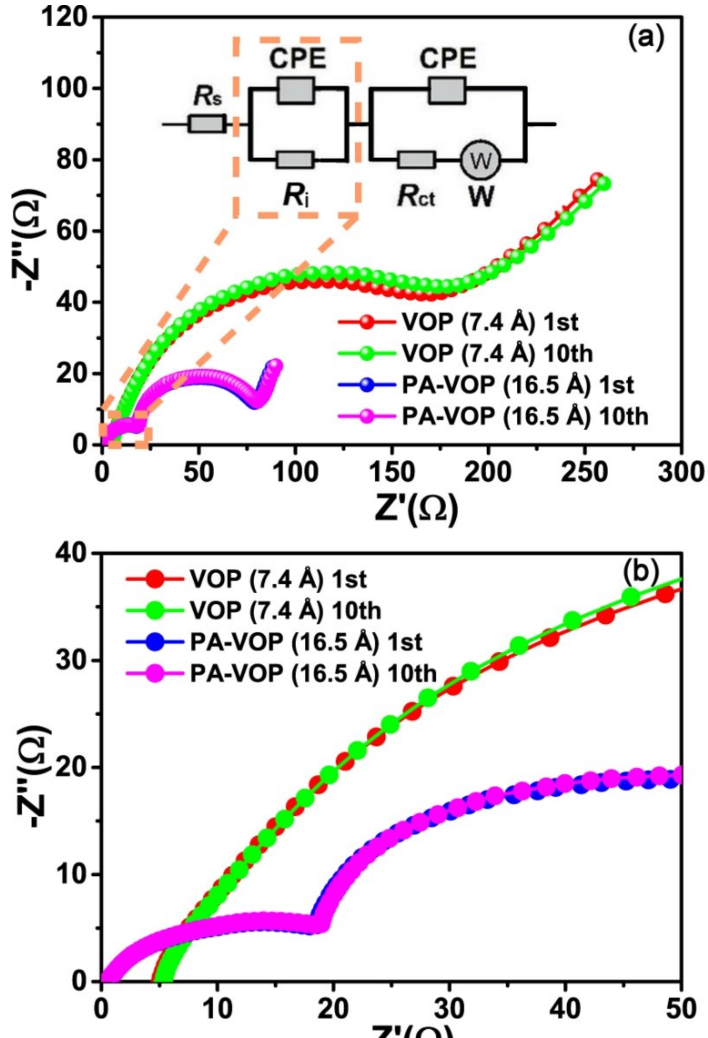

Fig. S15. Nyquist plots of pure VOP (7.4 Å) and PA-VOP (16.5 Å) composited cathode after several cycles.